

Anomalous Coiling of SiGe/Si and SiGe/Si/Cr Helical Nanobelts

Li Zhang, Elisabeth Ruh, and Detlev Grützmacher*

Laboratory for Micro- and Nanotechnology, Paul Scherrer Institute,
CH-5232 Villigen PSI, Switzerland

Lixin Dong, Dominik J. Bell, and Bradley J. Nelson

Institute of Robotics and Intelligent Systems, ETH Zurich,
CH-8092 Zurich, Switzerland

Christian Schönenberger

Institut für Physik, University of Basel, CH-4056 Basel, Switzerland

Received November 28, 2005; Revised Manuscript Received May 3, 2006

ABSTRACT

The fabrication of nanohelices by the scrolling of strained bilayers is investigated. It is shown that structure design is dominated by edge effects rather than bulk crystal properties such as the Young's modulus when the dimensions of the structures are reduced below 400 nm. SiGe/Si/Cr, SiGe/Si, and Si/Cr helical nanobelts are used as test structures. Dimensions of the belt width are reduced from 1.30 μm to 300 nm, and parameters controlling helicity angle, chirality, diameter, and pitch of the nanohelices are investigated. An anomalous scrolling direction deviating from the preferred $\langle 100 \rangle$ scrolling direction has been found for small structures. Making use of the anomalous scrolling, it is possible to fabricate three-dimensional helices with helicity angles less than 45° , which is advantageous for micro- and nanoelectromechanical systems.

A variety of nanostructures such as nanotubes, nanowires, and nanobelts have been extensively investigated in recent years because of their potential applications in several fields^{1–4} including sensors and actuators, nanoelectronics, micro- and nano-electromechanical systems (MEMS and NEMS), and optics. Among these structures, three-dimensional (3D) helices have potential applications for biosensors and gas sensors, cantilevers, resonators, and micromechanical components. Nanobelts and nanohelices have been synthesized from different materials, such as carbon,⁵ zinc oxide,^{6,7} and silicon carbide.⁸ Typically, the synthesis of these structures relies on spontaneous formation processes leading to a variety of sizes, orientations, and shapes of the structures.

Recently, the scrolling of strained semiconductor heterostructures has been applied to the fabrication of SiGe/Si and SiGe/Si/Cr helical nanobelts with controllable pitch, helicity, and diameter.⁹ The structures are formed by the stress-relieving coiling of patterned heterofilms.^{9–11} These free-standing helical structures produced from layered stacks, 20–60 nm thick, and stripe widths of more than 1 μm have proven to be robust and reproducible. The diameter of these structures is determined by the thickness and the strain of each of the individual films in the layer stack, whereas the scrolling direction is dominated by the Young's modulus,

which is strongly anisotropic in the strained Si/SiGe films. Thus, the coiling direction of SiGe/Si/Cr and SiGe/Si helical coils that are fixed at one end to the Si(001) substrate is along $\langle 100 \rangle$, the direction where Young's modulus is smallest. Previously we showed that for mesa lines oriented away from the $\langle 100 \rangle$ direction, the helicity angle θ (see Figure 1) of these helical nanobelts cannot be smaller than 45° .⁹ To use the helical nanobelts in nanoelectromagnets, nanoinductors, or nanosprings, it would be desirable if the helicity angle could be reduced sufficiently to allow for a significant increase of the magnetic flux density¹² or the flexibility.

For some applications it is advantageous to add a metal layer to the SiGe/Si bilayer. It has been shown that e-beam evaporated Cr supports the scrolling process¹³ and will increase the conductivity as well as the mechanical strength of the structure. As previously mentioned, the scrolling direction of SiGe/Si bilayer structures on a Si(001) surface is determined by the orientation of the smallest Young's modulus.¹¹ On the other hand, the amorphous (or polycrystalline) Cr layer has an isotropic Young's modulus. To analyze the scrolling direction of the SiGe/Si/Cr structure, the trilayer system can be divided into two bilayer parts, i.e., SiGe/Si and Si/Cr. The final scrolling direction can then be considered by combining these two components.

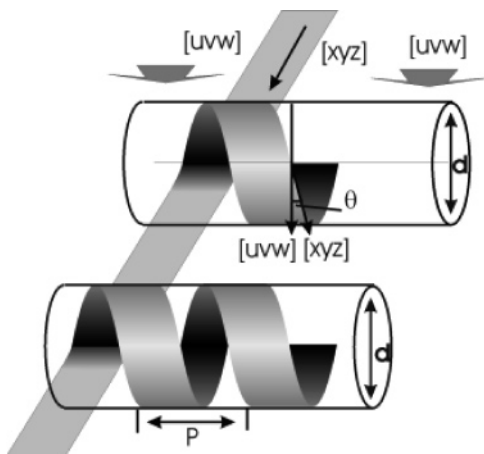


Figure 1. Schematic drawing of a helix formed by rolling-up of a stripe. The definitions of diameter d , pitch p , and helicity angle θ are presented in the figure where $p = \pi d \tan \theta$. The crystal orientation of the stripe is represented by $[xyz]$, and $[uvw]$ is defined as the scrolling direction. This helix shows a right-handed chirality.

In this paper, the formation of nanohelical structures from mesa lines less than $1 \mu\text{m}$ in width is investigated. Reducing the mesa line width increases the impact of edge effects on the scrolling process which may offer a path to overcome the restrictions on structure geometry due to bulk effects that occur from wide mesa lines. Therefore, this paper discusses in detail the impact of edge effects on chirality, scrolling direction, and diameter of SiGe/Si nanoscrolls as well as SiGe/Si/Cr helical nanobelts.

The p-type SiGe/Si heterofilms were grown by ultrahigh vacuum chemical vapor deposition (UHV-CVD) on Si(001). The Cr layers were deposited by e-beam evaporation. The initial planar trilayer structure contains an 11 nm thick SiGe layer with approximately 40% Ge, an 8 nm thick Si layer, and a 10 or 21 nm thick Cr layer. Details of the fabrication of the SiGe/Si/Cr stripe pattern and subsequent underetching using wet chemical etching have been described elsewhere.⁹ All stripes deviated by 5° or 10° from the $\langle 110 \rangle$ direction. The widths of the stripes were varied from 1.30 to $0.30 \mu\text{m}$ in steps of 100 nm. To fabricate the SiGe/Si stripe pattern, the Cr layer was removed by a Cl_2/CO_2 plasma etching process prior to wet etching. Subsequently the 3D structure was formed by wet chemical etching in an alkaline solution (3.7% NH_4OH). The samples were dried in a supercritical point dryer to greatly reduce adhesion to the substrate due to capillary forces.¹⁴

To study the scrolling behavior of Si/Cr structures, stripes of Si/Cr bilayers have been patterned into a “Siemensstern” (wagon wheel pattern¹⁵) having a rotational symmetry. These bilayers were deposited on a low-doped Si(100) substrate and consisted of a 35 nm thick Si layer heavily doped with boron and a 10 nm thick Cr top layer. After the mesa pattern was formed, scrolling was initiated by etching the substrate selectively in a 3.7% NH_4OH solution at room temperature.

After fabrication, the helical structures were inspected by field-emission scanning electron microscopy (FESEM, Zeiss SUPRA 55VP) to determine structural parameters. The definitions of the diameter d , pitch p , the chirality, and the helicity angle θ of the helical nanobelts are illustrated in

Figure 1. The geometrical relation between the pitch, the diameter, and the helicity angle of a helical nanobelt is described in ref 9.

Figure 2a–g shows scanning electron microscope (SEM) images of SiGe/Si/Cr helical nanobelts fabricated from mesa lines with the stripe width ranging from $1.3 \mu\text{m}$ (Figure 2a) to $0.7 \mu\text{m}$ (Figure 2g). All mesa lines are oriented $+10^\circ$ from the $[110]$ direction as indicated in Figure 2a. Helical coils produced from relatively wide stripes (1.30 and $1.20 \mu\text{m}$) show a right-handed chirality (Figure 2a,b), which is consistent with results previously reported.⁹ In this paper this type of helical coil is named an “ α -helix”. Reducing the stripe width to 1.1 and $1.0 \mu\text{m}$, both left- and right-handed chiralities occur in a single helix as depicted in parts c and d of Figure 2, respectively. This type of slightly disordered helical coil is named a “ β -helix” throughout this paper. The position along the coil in which the chirality of the helix changes is near the free end of the coil in Figure 2c, whereas the chirality changes close to the fixed end of the stripe for the helix with a smaller width (see Figure 2d). Also, the shape of the β -helix is often irregular, sometimes appearing disordered due to the confluence of the two competing chiralities. The width of the mesa lines is reduced to 0.9 , 0.8 , and $0.7 \mu\text{m}$ in parts e, f, and g of Figure 2, respectively. The helices formed from 0.9 and $0.8 \mu\text{m}$ wide mesa lines possess a left-handed chirality, the opposite chirality of those formed from wider mesa lines of the same orientation. This kind of helix is defined as a “ γ -helix”. Thus, three different regimes can be defined, broad mesa lines leading to right-handed helices, narrow lines resulting in left-handed helices, and a transition regime with disordered helices exhibiting both chiralities. A reverse orientation of mesa lines of -10° leads to opposite chiralities.

Moreover, not only the chirality but also the pitch and helicity angle change when the stripe width becomes smaller. Comparing the two “ γ -helices” shown in parts e and f of Figure 2, one can clearly observe in Figure 2f that the pitch and helical angle are smaller for the helix fabricated from the narrow mesa line ($0.9 \mu\text{m}$). Moreover when the mesa line is reduced to $0.7 \mu\text{m}$, the helical structure collapses into a multiturned ring structure, as depicted in Figure 2g. Here, both the helicity angle and the pitch go to zero. Consequently, by adjusting the stripe width for a given strained SiGe/Si/Cr layer stack, it is possible to control the pitch of the helical nanobelts. In particular, more tightly wound nanocoils can be designed and fabricated.

In previous work it was shown that the Cr layer deposited by e-beam evaporation is in tensile stress, thus enhancing the scrolling process.¹³ To study the impact of the Cr layer, SiGe/Si tubes were fabricated from the same sample using the same mask layout. After the mesa structures were fabricated, the Cr layer was removed by an RIE step, and subsequently, scrolling was initiated by wet chemical etching of the substrate. Interestingly, all of these stripes with a width in the range of 0.7 – $1.3 \mu\text{m}$ transformed into α -type helices. Figure 2h compares the result of a scrolling experiment using $0.7 \mu\text{m}$ wide mesa lines for a SiGe/Si/Cr layer stack and a SiGe/Si bilayer (inset of Figure 2h). Here the misalignment

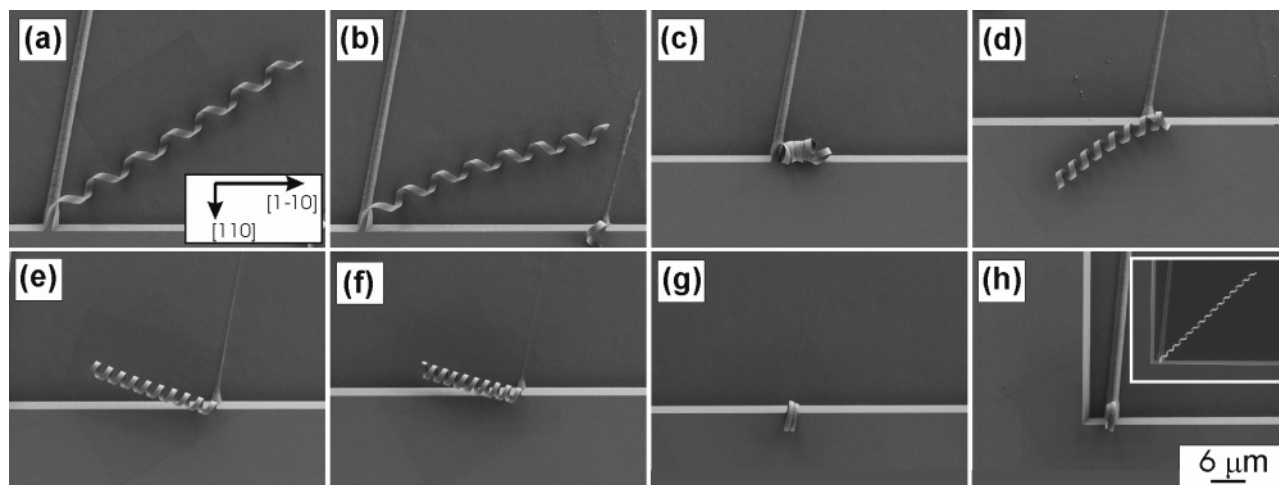


Figure 2. SEM top view images of $\text{Si}_{0.6}\text{Ge}_{0.4}/\text{Si}/\text{Cr}$ helical coils with layer thickness of 11/8/21 nm, except for the one in the inset of (h) which is without a Cr layer. The $\langle 110 \rangle$ orientation on the substrate is shown in (a) by black arrows. In (a–g) all stripes deviate 10° from the $\langle 110 \rangle$ direction, and the width of the stripes decreases stepwise from 1.30 to $0.70 \mu\text{m}$ with steps of 100 nm. Both nanobelts in (h) deviate 5° from $\langle 110 \rangle$. All images have the same scale bar.

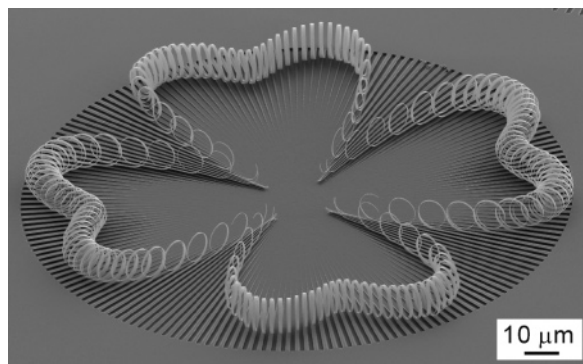


Figure 3. SEM image of 3D structures formed from a bilayer of p-type crystalline Si coated by amorphous Cr. The “ringlike” structure is formed after selective etching of the undoped Si substrate underneath.

angle was $+5^\circ$. Strikingly, the $\text{SiGe}/\text{Si}/\text{Cr}$ layers scroll into a multiwalled ring, whereas the SiGe/Si bilayer forms a right-handed helix. Therefore, to further reveal the effect of stripe width on the forming of $\text{SiGe}/\text{Si}/\text{Cr}$ helical nanobelts, it is necessary to investigate the influence of the Cr layer on the scrolling process.

To investigate the impact of the Cr separately, stripes of Si/Cr bilayers were prepared. Here the tensile strain of the Cr layer will initiate the scrolling process. For mesa lines oriented along the $[110]$ orientation, a transition from the $\langle 100 \rangle$ scrolling direction forms helices in the $\langle 110 \rangle$ scrolling direction, which forms rings. This was also observed in Si/Cr bilayers when the mesa stripe width was reduced from 3 to $0.5 \mu\text{m}$.¹⁶ Here, wagon wheel patterns were investigated consisting of tapered mesa lines with a width of $1.4 \mu\text{m}$ in the outermost region and 60 nm close to the center of the wheel. Figure 3 shows an SEM image of the rolled-up Si/Cr stripes obtained from the wagon wheel pattern. Clearly, without exception all these stripes are coiled in the direction along the longitudinal axis of stripe. Comparing the experiments done with $\text{SiGe}/\text{Si}/\text{Cr}$, SiGe/Si and Si/Cr indicates that the Cr layer is responsible for the change in pitch observed in Figure 2. The strained polycrystalline or amorphous Cr

layer can be assumed to be an isotropic material, thus inducing no preferential scrolling direction. However, the underlying Si layer is stretched by the scrolling process. This Si layer has an anisotropic Young’s modulus which should effect the preferred scrolling direction. However, experimental observation for thin lines demonstrates an additional effect which apparently overrides the effect of the anisotropic Young’s modulus.

In addition, it has been observed that for thinner Cr layers, the stripe width necessary to switch the helicity of the $\text{SiGe}/\text{Si}/\text{Cr}$ coil from α to β and γ types is reduced. For $\text{Si}_{0.6}\text{Ge}_{0.4}/\text{Si}$ bilayer structures without Cr, only α types have been found for mesa widths greater than 700 nm. Consequently, for the $\text{Si}_{0.6}\text{Ge}_{0.4}/\text{Si}$ bilayers the width of the mesa lines was reduced from 700 to 300 nm. The misaligned angle of all stripes is 5° from $\langle 110 \rangle$. The experimental results show the helices formed by the 400 and 300 nm wide lines are γ type and exhibited a strong decrease in pitch, indicating a pronounced deviation from the $\langle 100 \rangle$ scrolling direction determined by the Young’s modulus. Thus, the same pattern for the SiGe/Si bilayer can be found as previously obtained for the $\text{SiGe}/\text{Si}/\text{Cr}$ and Si/Cr hybrid structures when the stripe width becomes sufficiently narrow.

The experimental observations are summarized in Figure 4, showing the dependence of the diameter and the helicity angle on the width of the mesa lines, respectively. Parts a and b of Figure 4 compare the diameter of $\text{SiGe}/\text{Si}/\text{Cr}$ helices with 21 and 10 nm Cr to those of SiGe/Si helices for lines oriented 5° (Figure 4a) and 10° (Figure 4b) from the $[110]$ direction. According to Suo et al.¹⁷ and Grundmann,¹⁸ the diameter d of the SiGe/Si helix can be expressed as

$$d = (E_{\text{Si}}^2 d_1^4 + 4E_{\text{Si}}E_{\text{SiGe}}d_1^3d_2 + 6E_{\text{Si}}E_{\text{SiGe}}d_1^2d_2^2 + 4E_{\text{Si}}E_{\text{SiGe}}d_1d_2^3 + E_{\text{SiGe}}^2d_2^4) / (3\epsilon E_{\text{Si}}E_{\text{SiGe}}d_1d_2(d_1 + d_2)(1 + \nu)) \quad (1)$$

From eq 1, the diameter of the helix is determined not only by layer thickness (d_1 , d_2), Young’s modulus E , and

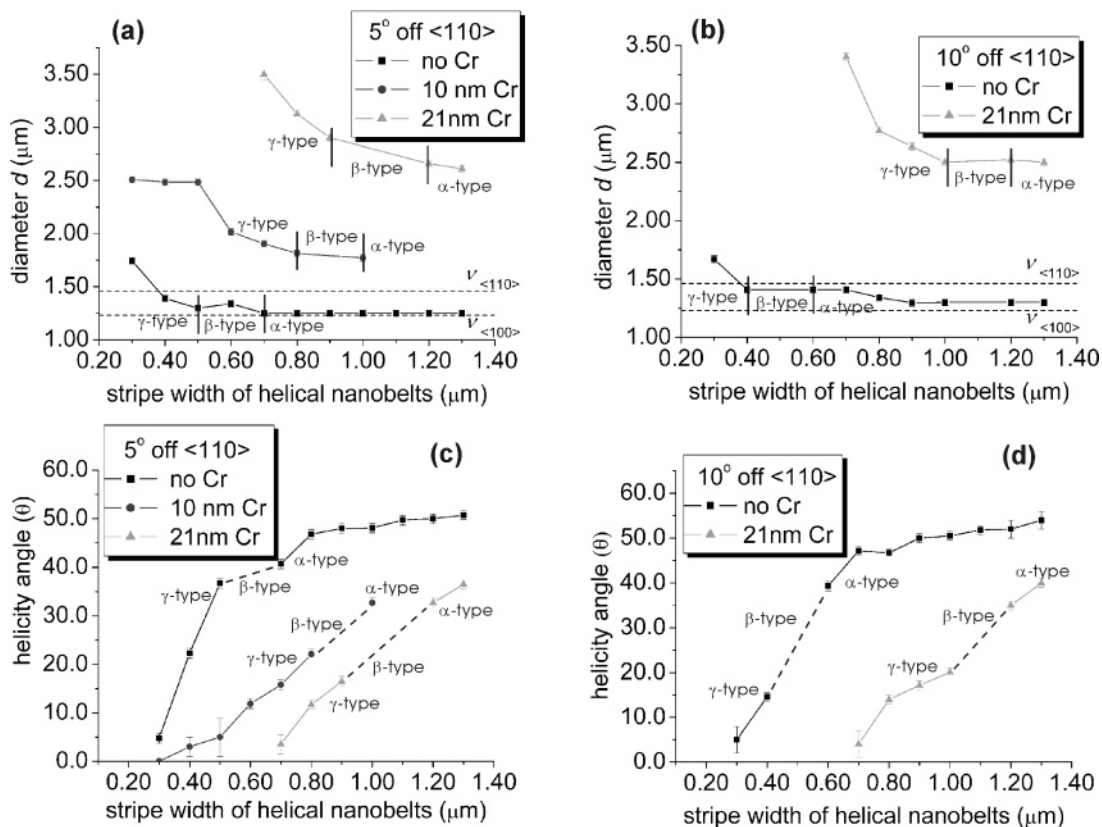


Figure 4. Statistical curves showing the relationship between the stripe width and the diameter d for $\text{Si}_{0.6}\text{Ge}_{0.4}/\text{Si}$ and $\text{Si}_{0.6}\text{Ge}_{0.4}/\text{Si}/\text{Cr}$ nanocoils. (a) Stripes deviate 5° from $\langle 110 \rangle$. (b) Stripes deviate 10° from $\langle 110 \rangle$. Dashed lines give the calculated diameter of helical nanobelts which scroll along the $\langle 100 \rangle$ and $\langle 110 \rangle$ directions. (c, d) The relationship of the stripe width and the helicity angle (θ) for $\text{Si}_{0.6}\text{Ge}_{0.4}/\text{Si}$ and $\text{Si}_{0.6}\text{Ge}_{0.4}/\text{Si}/\text{Cr}$ nanocoils. (c) Stripes deviate 5° from $\langle 110 \rangle$. (d) Stripes deviate 10° from $\langle 110 \rangle$. Dashed lines represent the β -helix region, which has a mixed chirality and irregular helicity.

lattice mismatch ϵ but also by Poisson's ratio ν of the Si layer. When the coiling direction deviates from $\langle 100 \rangle$ to the stripe orientation $\langle hk0 \rangle$, the Poisson's ratio of the Si layer decreases,¹⁹ leading to an increase in diameter. However, since $0.07 \leq \nu_{\text{Si}} \leq 0.27$ on $\text{Si}(001)$, the increase in diameter should be bounded by the limits of the Poisson's ratio.²⁰ The broken horizontal lines in Figure 4a,b indicate the maximum ($\nu_{\langle 110 \rangle}$) and minimum ($\nu_{\langle 100 \rangle}$) calculated diameter when the extremes of the Poisson's ratio and corresponding Young's modulus are used. Figure 4 demonstrates that α -helices formed by wide mesa lines of the SiGe/Si bilayers are close to the predictions for scrolling along the $\langle 100 \rangle$ direction. Also, in the transition regime of β helical nanobelts the diameter is within the limitations given by the Poisson's ratio. However, when the γ -type helical nanobelts appear, the diameter increases dramatically and the diameter of helices formed from narrow mesa lines deviates significantly from the model.

Parts c and d of Figure 4 give the relationship between the measured helicity angle θ and the stripe width for the same helices previously discussed in the context of Figure 4a,b. Due to the preferred scrolling direction along the $\langle 100 \rangle$ direction in combination with the anisotropic etching, the helicity angles of stripes with a misaligned angle of 5° (Figure 4c) or 10° (Figure 4d) from $\langle 110 \rangle$ should produce coils with helicity angles of 50° and 55° , respectively.⁹ Within the experimental error of the SEM measurements,

this is confirmed by the α -helices. However, the experimental results for β - and γ -type helices clearly deviate from this prediction. It is evident from Figure 4c,d that deviation increases with decreasing stripe width and increasing Cr layer thickness. Furthermore, once the γ -type helix appears, the helicity angle linearly decreases until rings form from very narrow mesa lines.

We attribute the phenomena shown in Figure 4 to the increasingly dominating edge effects of narrow stripes. At the edges, part of the stress incorporated in the stripe^{20,21} will relax and, thus, decrease the strain ϵ . Finite element method (FEM) simulations (ABAQUS) were used to validate the prediction. For the simulations, a 300 nm wide and 1000 nm long SiGe/Si bilayer stripe with a 8 nm thick Si layer and a 11 nm SiGe layer were used. As the length should have no influence on the strain (if the length is long compared to the width), the simulation was not done with lengths of $100 \mu\text{m}$ in favor of having many small and accurate finite elements.

For orthotropic crystal systems ABAQUS uses engineering constants for the elastic properties of the materials (Young's moduli, Poisson ratios, shear moduli). These constants are related to the three material main axes being mutually orthogonal and perpendicular to the mirror planes of the crystal system. Due to the diamond structure of Si/SiGe there are no such material main axes: the axes $X = (1-10)$ and $Y = (110)$ of the stripe fulfill this condition, whereas their

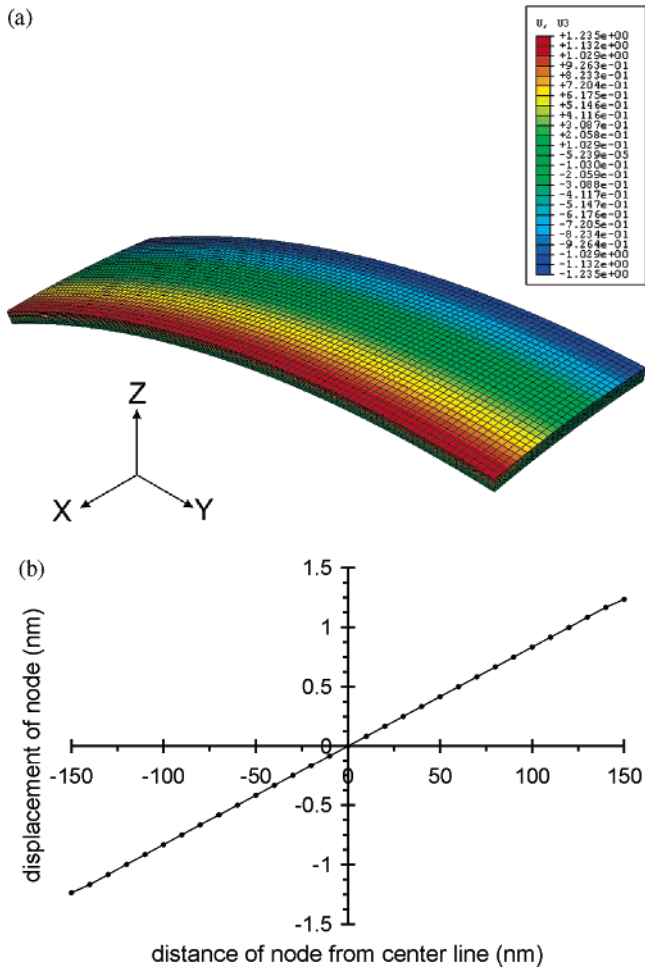


Figure 5. (a) Displacement contour plot of the FEM of the SiGe/Si bilayer stripe along the direction $X = (1-10)$. The SiGe/Si bilayer stripe has a thickness of 19 nm (8 nm Si/11 nm SiGe), a width of 300 nm, a length of 1 μm , and is aligned to $\langle 110 \rangle$. In the simulation, the top layer is the SiGe layer for easy inspection. (b) Line plot of the displacement in the X -direction of the FEM nodes from the stripe front top edge.

third related axes $Z = (001)$ does not. However, the most reliable solution takes $X = (1-10)$, $Y = (110)$, and $Z = (001)$ for the material main axes system. The values of Young's moduli, Poisson ratios, and shear moduli related to this main axes system were taken from ref 19.

According to the FEM simulations, the displacement of the nodes of the finite elements increases linearly with the distance from the center line of the stripe. For instance, the lattice displacement in the X -direction at the edges of the SiGe stripe is about 1.24 nm at each side of the stripe as shown in Figure 5. Thus, the FEM simulations show that the stress in the SiGe layer is partially relaxed along the X -direction.

The strain condition in the helical nanobelts is quite complex. The scrolling process relaxes the strain only in the direction of scrolling where it does not affect the strain in the perpendicular direction. The FEM simulations show that at the edges the strain will partially relax in the direction perpendicular to the longitudinal axes of the mesa. This relaxation process does not depend on the width of the mesa line used for the helix fabrication. However, the ratio between

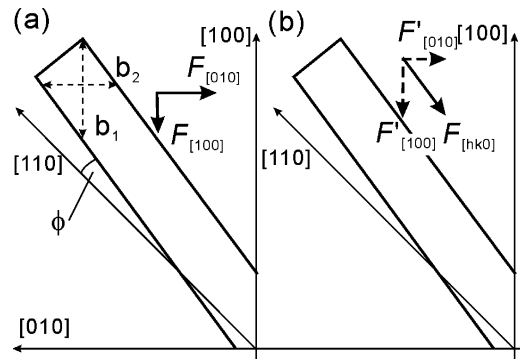


Figure 6. A schematic drawing for the explanation of the change of the chirality. The SiGe/Si stripe has ϕ degree from $[110]$. (a) The lengths b_1 and b_2 are the length of the lines that intersect the mesa line along $[100]$ and the $[010]$, respectively. (b) $F_{[hk0]}$, which is induced by asymmetrical stress relaxation, can be decomposed into $F'_{[010]}$ and $F'_{[100]}$, and $F'_{[010]} < F'_{[100]}$.

strained and relaxed material will decrease with decreasing stripe width. It appears obvious that stress relaxation leads to increasing diameters of helical nanobelts with decreasing stripe width (Figure 4a,b), whereas an explanation of chirality change requires a detailed discussion of the phenomena related to the stress relaxation.

For conventional helical nanobelts,⁹ i.e., those in which edge effects can be neglected, the compressive forces along $[100]$ and $[010]$ can be written as

$$F_{[100]} = \frac{1}{2} \delta_{[100]} b_2 d_2 \left(\frac{d_1 E_{\text{Si}}}{d_1 E_{\text{Si}} + d_2 E_{\text{SiGe}}} \right) \quad (2)$$

$$F_{[010]} = \frac{1}{2} \delta_{[010]} b_1 d_2 \left(\frac{d_1 E_{\text{Si}}}{d_1 E_{\text{Si}} + d_2 E_{\text{SiGe}}} \right) \quad (3)$$

where δ is the stress in SiGe layer due to the lattice mismatch of the SiGe layer to the Si layer, E is the effective Young's modulus,²² b is the length over which the scrolling process occurs, and d_1 and d_2 are the thicknesses of the Si and SiGe layers, respectively. The $F_{[100]}$ and $F_{[010]}$ along the preferred scrolling orientations $[100]$ and $[010]$ will be different for a mesa line slightly tilted from the $\langle 110 \rangle$ direction, which becomes clear in Figure 6a. Here the lengths b_1 and b_2 are the lengths of the lines that intersect the mesa line along the $[100]$ and the $[010]$, respectively. The forces are proportional to b_2 and b_1 . A tensile force with the same magnitude as described by eqs 2 and 3 acts on the Si layer. This pair of forces between the SiGe and Si layers will generate a bending moment M , which can be expressed by ref 23

$$M = F_{\text{SiGe}} \left(\frac{d_1 + d_2}{2} \right) \quad (4)$$

If the stripe is ϕ degrees from $\langle 110 \rangle$, as defined in Figure 6a, b_1 becomes larger than b_2 . Then the force $F_{[010]}$ will be larger than $F_{[100]}$, which leads to a different bending moment along the two $\langle 100 \rangle$ directions. This model nicely describes the observations gathered for broad mesa lines (α -helix),

which also have been previously reported.^{9,23} When the stripe becomes narrower, the difference in absolute values between b_1 and b_2 becomes smaller and thus the difference for the forces $F_{[010]}$ and $F_{[100]}$ will become smaller as well. However, the reverse of the scrolling direction (chirality) to form a γ -type helix still requires a driving force along a direction other than the original [100]. This force arises from the perpendicular stress relaxation at the two edges of a stripe pattern. The FEM analyses show that the crystalline structure near the edge can relax perpendicular to the mesa line since the atoms at the rim can move outward, whereas little or no relaxation will occur parallel to the mesa line. Consequently, this asymmetrical relaxation process at the rim of the mesa line will induce a force $F_{[hk0]}$, which is directed along the mesa line, as shown in Figure 6b. The force $F_{[hk0]}$ can be decomposed into forces $F'_{[010]}$ and $F'_{[100]}$ as illustrated in Figure 6b. Notably, for the same orientation angle ϕ of the mesa line shown in parts a and b of Figure 6, the force $F_{[010]}$ is larger than $F_{[100]}$, whereas $F'_{[010]}$ is smaller than $F'_{[100]}$. The difference between $F'_{[010]}$ and $F'_{[100]}$ is independent of the mesa line widths, whereas the difference of $F_{[010]}$ and $F_{[100]}$ decreases with the width of the mesa line. Thus, it is proposed that the change in chirality occurs when

$$|F_{[010]} - F_{[100]}| < |F'_{[010]} - F'_{[100]}| \quad (5)$$

Furthermore, adding a strained isotropic film, such as the Cr film, will increase the effect of $F_{[hk0]}$,²¹ which is in perfect agreement with the experimental observations. The change in chirality occurs at wider mesa line widths if a thicker Cr layer is incorporated in the layer stack (Figure 4a,b).

Using this model, the impact of the mesa line width on the pitch (Figure 2e,f), i.e., on the helicity angle (Figure 4c,d), is also explained. The pitch decreases; i.e., the helicity angle decreases, with decreasing mesa line widths. If the SiGe/Si/Cr or SiGe/Si stripe width becomes narrow enough, the scrolling direction is near the stripe longitudinal axis $[hk0]$ instead of the $\langle 100 \rangle$ direction. Due to the relaxation of strain perpendicular to the mesa line orientation, the material at the edges of the mesa line can be considered as harboring predominantly uniaxial strain along the mesa line. This uniaxial strain component will induce the force $F_{[hk0]}$, i.e., a moment for scrolling in the direction parallel to the mesa line. Consequently, in the mesa lines used for the fabrication of helical nanobelts, a biaxial strain condition in the center of the mesa line and a uniaxial strain condition at the sides of the mesa line exist. The latter is independent of the mesa line width, whereas the former decreases with line width. The area under biaxial strain induces a preferred scrolling direction along $\langle 100 \rangle$ directions, whereas the uniaxial strain at the sides prefers scrolling parallel to the mesa line, i.e., both forces $F_{\langle 100 \rangle}$ along one of the $\langle 100 \rangle$ directions and the force $F_{[hk0]}$ at the mesa sides must sum together to determine the scrolling direction. For narrow lines this leads to a reduction of the helicity angle, i.e., the scrolling direction is shifted from the $\langle 100 \rangle$ directions toward the $[hk0]$ orientation of the mesa line. The experimental results suggest that for

very narrow Si/SiGe mesa lines (< 300 nm) $F_{[hk0]}$ will become dominant and the structure scrolls into a multiwall ring along the mesa line. It should be noted that this change in scrolling direction away from the $\langle 100 \rangle$ direction will also lead to an increase in the diameter.

On the basis of our results it can be also concluded that when the stripe width is decreased, the Cr-coated helices will change the nature of helicity (α , β , and γ) at a larger stripe width than those without Cr. The Cr film can be considered to be isotropic, thus it will not induce a preferred scrolling direction. However, the strained Cr film will relax at the edges as well, thus adding uniaxially strained material at the edges without adding a moment in the $\langle 100 \rangle$ directions, i.e., $F_{[hk0]}$ increases whereas $F_{\langle 100 \rangle}$ remains the same.

In conclusion, anomalous scrolling of SiGe/Si and SiGe/Si/Cr helical nanobelts (β and γ types) has been observed. The nature of the helicity of the nanocoils differs from conventional helical nanobelts (α helix).⁹ Two factors dominate the chirality of a helix formed on Si(100). The first is the different bending moment between the two $\langle 100 \rangle$ directions, which depends on the orientation of the mesa line. The bending moment of a stripe can be affected locally by tailoring the pattern shape. The second factor is the impact of strain relaxation at the sidewalls of the mesa lines, which leads to an asymmetrical lattice distortion in the plane of the films and, in turn, to a uniaxial strain component along the mesa line. This uniaxial strain component is responsible for the deviation of the preferred $\langle 100 \rangle$ scrolling direction for Si/SiGe bilayer films on Si(100) substrates obtained for narrow mesa lines. The anomalous coiling of narrow mesa lines can be used to tune the chirality, pitch, and helical angle for nanohelices. Adding films with an isotropic Young's modulus such as amorphous or polycrystalline metal can also be used to tailor these parameters. With this technique, helical nanobelts with a helical angle of less than 10° can be achieved, which is much smaller than the previously reported minimum 45° given by the preferred $\langle 100 \rangle$ scrolling direction. These techniques will create new opportunities for the design and fabrication of nanocomponents having applications in MEMS and NEMS.

Acknowledgment. The authors thank Eugen Deckardt and Anja Weber (PSI) for their technical support. This work is supported by the Swiss National Science Foundation and the ETH-Zurich.

References

- (1) Iijima, S. *Nature* **1991**, *354*, 56.
- (2) Cui, Y.; Lieber, C. M. *Science* **2001**, *291*, 851.
- (3) Wu, Y.; Xiang, J.; Yang, C.; Lu, W.; Lieber, C. M. *Nature* **2004**, *430*, 61.
- (4) Wang, Z. L. *Nanowires and Nanobelts: Materials, Properties and Devices*; Kluwer Academic: Boston, MA, 2003.
- (5) Amelinckx, S.; Zhang, X. B.; Bernaerts, D.; Zhang, X. F.; Ivanov, V.; Nagy, J. B. *Science* **1994**, *265*, 635.
- (6) Kong, X. Y.; Wang, Z. L. *Nano Lett.* **2003**, *3*, 1625.
- (7) Gao, P. X.; Ding, Y.; Mai, W. J.; Hughes, W. L.; Lao, C. S.; Wang, Z. L. *Science* **2005**, *309*, 1700.
- (8) Zhang, D. Q.; Alkhateeb, A.; Han, H.; Mahmood, H.; McIlroy, D. N. *Nano Lett.* **2003**, *3*, 983.

- (9) Zhang, L.; Deckardt, E.; Weber, A.; Schönenberger, C.; Grützmacher, D. *Nanotechnology* **2005**, *16*, 655.
- (10) Prinz, V. Ya.; Seleznev, V. A.; Gutakovskiy, A. K.; Chehovskiy, A. V.; Preobrazhenskii, V. V.; Putyato, M. A.; Gavrilova, T. A. *Physica E* **2000**, *6*, 828.
- (11) Golod, S. V.; Prinz, V. Ya.; Mashanov, V. I.; Gutakovskiy, A. K. *Semicond. Sci. Technol.* **2001**, *16*, 181.
- (12) Bell, D. J.; Dong, L. X.; Sun, Y.; Zhang, L.; Nelson, B. J.; Grützmacher, D. *Proc. IEEE Conf. Nanotechnol., 5th* **2005**, 303.
- (13) Golod, S. V.; Prinz, V. Ya.; Wägli, P.; Zhang, L.; Kirfel, O.; Deckardt, E.; Glaus, F.; David, C.; Grützmacher, D. *Appl. Phys. Lett.* **2004**, *84* (17), 3391.
- (14) Seleznev, V.; Yamaguchi, H.; Hirayama, Y.; Prinz, V. Ya. *Jpn. J. Appl. Phys.* **2003**, *42*, 791.
- (15) Seidel, H. Csepregi, L.; Heuberger, A.; Baumgärtel, H. *J. Electrochem. Soc.* **1990**, *137* (11), 3612.
- (16) Zhang, L.; Dong, L. X.; Bell, D. J.; Nelson, B. J.; Schönenberger, C.; Grützmacher, D. *Microelectron. Eng.* **2006**, *83*, 1237.
- (17) Suo, Z.; Ma, E. Y.; Gleskova, H.; Wagner, S. *Appl. Phys. Lett.* **1999**, *74* (8), 1177.
- (18) Grundmann, M. *Appl. Phys. Lett.* **2003**, *83* (12), 2444.
- (19) Wortman, J. J.; Evans, R. A. *J. Appl. Phys.* **1965**, *36*(1), 153.
- (20) Shen, Y. L.; Suresh, S.; Blech, I. A. *J. Appl. Phys.* **1996**, *80* (3), 1388.
- (21) Gouldstone, A.; Shen, Y. L.; Suresh, S.; Thompson, C. V. *J. Mater. Res.* **1998**, *13* (7), 1956.
- (22) Huang, M.; Boone, C.; Roberts, M.; Savage, D. E.; Lagally, M. G.; Shaji, N.; Qin, H.; Blick, R.; Nairn, J. A.; Liu, F. *Adv. Mater.* **2005**, *17*, 2860.
- (23) Tsui, Y. C.; Clyne, T. W. *Thin Solid Films* **1997**, *306*, 23.

NL052340U